Surface complexation modeling of Cd(II) sorption to montmorillonite, bacteria, and their composite

Ning Wang[1,2]*, Huihui Du[1,2]*, Qiaoyun Huang[1,2]**, Peng Cai[1,2], Xingmin Rong[2] and Wenli Chen[1,**]

[1] State Key Laboratory of Agricultural Microbiology, Huazhong Agricultural University, Wuhan 430070, China.

[2] Key Laboratory of Arable Land Conservation (Middle and Lower Reaches of Yangtze River), Ministry of Agriculture, College of Resources and Environment, Huazhong Agricultural University, Wuhan 430070, China.

*These authors contributed equally to this work.

**Corresponding author: Q. Huang, E-mail: qyhuang@mail.hzau.edu.cn; W. Chen, wlchen@mail.hzau.edu.cn; Tel: +86-27-87671033; Fax: +86-27-87280670

Abstract

Surface complexation modeling (SCM) has emerged as a powerful tool for simulating heavy metal adsorption processes on the surface of soil solid components under different geochemical conditions. The component additivity (CA) approach is one of the strategies that have been widely used in multi-component systems. In this study, potentiometric titration, isothermal adsorption, zeta potential measurement, and extended X-ray absorption fine structure (EXAFS) spectra analysis were conducted to investigate Cd adsorption on 2:1 clay mineral montmorillonite, on Gram-positive bacteria *Bacillus subtilis*, and their mineral-organic composite. We developed constant capacitance models (CCM) of Cd adsorption on montmorillonite, bacterial cells, and mineral-organic composite. The adsorption behavior of Cd on the surface of the composite was well explained by CA-SCM. Some deviations were observed from the model simulations at pH < 5, where the values predicted by the model were lower than the experimental results. The Cd complexes of X_2Cd, $SOCd^+$, $R-COOCd^+$, and $R-POCd^+$ were the predominant species on the composite surface over the pH range of 3 to 8. The distribution ratio of the adsorbed Cd between montmorillonite and bacterial fractions in the composite as predicted by CA-SCM closely coincided with the estimated value of EXAFS at pH 6. The model could be useful for the prediction of heavy metals distribution at the interface of multicomponents and their risk evaluation in soils and associated environments.

Keywords: montmorillonite, bacteria, composite, Cd(II), sorption, modeling

1. Introduction

Anthropogenic activity and industrialization release large quantities of heavy metals into soils (Fomina and Gadd, 2014; He and Chen, 2014). The interactions between soil solid components and heavy metals in complex natural systems should be understood in order to predict their transport and fate. Surface complexation modeling (SCM) is a powerful tool for describing adsorption processes and mechanisms under different geochemical conditions (Dong and Wan, 2014; Wang and Giammar, 2013). SCM has been adopted to simulate the adsorption of heavy metals on the surface of soil solid components such as kaolinite (Angove et al., 1997), montmorillonite (Akafia et al., 2011; Benedicto et al., 2014; Bradbury et al., 2005; Ikhsan et al., 2005; Soltermann et al., 2014), magnetite (Kim et al., 2012), manganese oxide (Wang et al., 2013), fulvic and humic acid (Christl et al., 2001; Koopal et al., 2005; Milne et al., 2003), natural organic matter (Koopal et al., 2005; Gustafsson et al., 2014), and bacteria (Borrok and Fein, 2005; Borrok et al., 2004; Daughney et al., 2001; Fein et al., 1997; Kenney and Fein, 2011; Liu et al., 2013; Moon and Peacock, 2011).

Soil solid components, which include bacteria and clay minerals, often exist as composites in natural environments. The component additivity (CA) approach has been widely used in the application of surface complexation models for describing heavy metal adsorption on mixtures and on the composites of soil solid components. The component additivity-diffuse layer model (CA-DLM) has been successfully applied to model the adsorption of Co^{2+} (Landry et al., 2009) and Pb^{2+} (Reich et al.,

72   2010), on mixtures of hydrous ferric oxide (HFO) and quartz with kaolinite. Dong and

73   Wan (2014) indicated that the CA-SCM can provide excellent predictions for uranium

74   (VI) adsorption on quartz-sand dominated sediments. Fowle and Fein (1999)

75   concluded that the CA approach can be used to model the adsorption of Ca^{2+}, Cu^{2+},

76   Cd^{2+}, and Pb^{2+} on mixtures of *Bacillus licheniformis* and *B. subtilis*. Additionally, CA

77   could successfully describe Cd, Co, Sr, and Zn adsorption onto the mixtures of 10

78   species of Gram-positive bacteria (Yee and Fein, 2001). For the mixtures of minerals

79   and organic systems, the extended constant capacitance model was used to depict

80   Cd^{2+} adsorption onto goethite, kaolinite, and muloorina illite in the presence of citric

81   acid (Lackovic et al., 2004a,b). The linear additivity model has succeeded in

82   predicting Cu^{2+} adsorption, but has failed to simulate Ca^{2+} adsorption on goethite in

83   the presence of fulvic acid (Weng et al., 2008). The adsorption of Cd^{2+} onto

84   *Comamonas spp.*–ferrihydrite composite could be accurately predicted by the addition

85   of the reaction between end-member ferrihydrite and bacteria (Song et al., 2009).

86   However, the amount of Cd^{2+} adsorption onto the composite was up to 10% lower

87   than that predicted by the additive approach. In the study of Alessi and Fein (2010)

88   the CA approach was applied to describe the extent of Cd adsorption on the surface of

89   two- and three-component mixtures of *B. subtilis* cells, HFO, and kaolinite at various

90   mass ratios in the presence of acetate. The models matched well with experimental

91   data in the absence of acetate, whereas they underestimated Cd adsorption in the

92   presence of acetate. Moon and Peacock (2013) found that Cu adsorption behavior on

93   ferrihydrite–*B. subtilis* composites with ferrihydrite as the major component can be

94   modeled by a component additivity approach. By contrast, composites with a majority

95   of bacteria component cannot be simulated by a component additivity approach, and

96   significant deviations were observed.

97   Previous studies concerning surface complexation models have mainly focused

98   on heavy metal adsorption by individual minerals or bacteria or mineral–organics and

99   metal oxide–bacteria composites. To the authors' knowledge, no SCM investigation

100   using 2:1 clay mineral–bacteria composites, has been performed. Montmorillonite, a

101   representative of the 2:1 phyllosilicates, exhibits large specific surface area and high

102   cation exchange capacity, which make it an effective adsorbent for heavy metals. The

103   clay mineral is widely distributed in a variety of soils in temperate zone. The model

104   developed in clay mineral–bacteria composites will provide insights into the

105   behaviors of heavy metals in contaminated soils of these regions. Thus, in this study,

106   we first develop surface complexation models for Cd adsorption on end-member 2:1

107   clay mineral montmorillonite, Gram-positive bacteria *Bacillus subtilis*, and finally

108   their mineral-organic composite by using the component additivity (CA) approach.

109   Moreover, linear combination fitting of the extended X-ray absorption fine structure

110   (EXAFS) spectra were applied to verify the distribution ratio of Cd between different

111   components derived from CA-SCM.

112

113   **2. Materials and Methods**

114

115   **2.1. Adsorbent and Reagent**

116   Montmorillonite, (Sanding Group Co. Ltd., Shaoxing, Zhejiang, China), was

117   prepared following previously outlined procedures (Hong et al., 2012; 2013). The

118   clays were oxidized using H_2O_2 (30%) to remove any residual organic matters. The <

119   2 μm colloidal fractions were isolated through sedimentation. The specific surface

120   area, determined by the BET method (N_2 adsorption), was found to be 60.2 m^2 g^{-1}.

121   Previous study showed that a particle was estimated to be formed of nearly 20 stacked

122   layers in the dehydrated state used in the gas adsorption experiment (BET' method),

123   whereas it was estimated to be composed of only 1 or 2 layers in aqueous suspension

124   (Tournassat et al., 2003). Thus, the values derived from BET' method usually

125   underestimate the actual total surface area in aqueous. Herein, we set the SSA of

126   montmorillonite to be 800 m^2 g^{-1}, and the detailed processing procedures are shown in

127   Supporting Information.

128   The test bacteria used in this study came from the aerobic Gram-positive species

129   *B. subtilis*, which were obtained from the State Key Laboratory of Agricultural

130   Microbiology. The microorganisms were inoculated into 10 mL LB medium and

131   cultured for 7 h at 28 ℃ to reach the exponential phase with an optical density of 1.4

132   at 600 nm (OD600 nm). Subsequently, 2 mL of the resulting bacterial suspension was

133   transferred to 200 mL LB medium for another 18 h inoculation ($OD_{600nm}=2.7$) to

134   reach the mid-exponential phase. Cells were pelleted by centrifugation at

135   approximately 7200 *g* for 5 min and rinsed three times in ultrapure water. The ratio of

136   the wet weight to dry (60 ℃ in drying oven) weight of the biomass is 9:1. The

137   biomass mentioned in this paper all refer to dry weight.

138   Montmorillonite and the bacterial cells were suspended in 0.01 M $NaNO_3$ to

139 produce the suspensions that were used in the experiments. The

140 montmorillonite–bacteria composite was prepared following a montmorillonite: *B.*

141 *subtilis* mass ratio of 7:1 to produce suspensions (4 h, 28 ℃). The resultant

142 montmorillonite–bacteria composite suspensions were used for subsequent

143 experiments. Preliminary isothermal adsorption (pH 8) of bacteria to montmorillonite

144 results showed that the maximum adsorption predicted by Langmuir equation was

145 approximately 0.14 g (dry cell)/ g (clay) which was equal to a mass ratio (clay to

146 bacteria) of 7:1 (Supporting Information, Fig. S1). Clearly adsorption of bacteria on

147 montmorillonite decreased with the increase of pH, thus bacteria can be completely

148 adsorbed by montmorillonite to a large extent in all experimental conditions (pH

149 3–8.5) at this ratio. The bacterial cells were remain intact under the experimental

150 condition (see AFM images of the Supporting Information, Fig. S2).

151   Analytical reagent grade chemicals were used throughout the study. $Cd(NO_3)_2$

152 was used to prepare 178.0 μmol L^{-1} Cd(II) stock solution. Water was Milli-Q reagent

153 grade.

154

155 **2.2. Zeta potential analysis**

156   Zeta potential analysis was conducted to study the surface charge properties of

157 montmorillonite, *B. subtilis,* and montmorillonite–*B. subtilis* composite. Suspensions

158 were prepared the same as section 2.1, over the pH range of 3 to 8. Samples were

159   injected into a zeta potential analyzer (Zetaplus90, Brookhaven), and measured in

160   triplicate.

2.3. Potentiometric titrations

162   Titration experiments were performed (in duplicate) according to the procedures

163   described by Fein et al. (2005). The suspensions (1 g L^{-1}, 40 mL) of montmorillonite

164   and *B. subtilis* and the composite in 0.01 M $NaNO_3$ were placed in a sealed titration

165   vessel maintained under a positive pressure of N_2. Titrations were conducted using an

166   automatic potentiometric titrator (Metrohm titrator 836, Switzerland). Each

167   suspension was first titrated to pH 3 by using 0.1136M HNO_3 solutions and then to

168   pH 8.5 by using 0.0976 M NaOH. At each titration step, a stability of 0.01 mV S^{-1} was

169   attained before adding the next drop of the titrant.

170   Gran plot was adopted to determine the specific volume of titrant added at the

171   equivalence point (Ve) and to derive the total H^+ concentration (TOTH) (Chu et al.,

172   2002; Du et al., 1997; Liu et al., 1999; Liu et al., 2013).

173   The values for the Gran function (G) were calculated as follows:

174   On the acidic side: $G_a = (V_0 + V_{at} + V_b) \times 10^{-pH} \times 100$

175   On the alkaline side: $G_b = (V_0 + V_{at} + V_b) \times 10^{-(13.8-pH)} \times 100$

176   Gran plots for titration data on montmorillonite and *B. subtilis* are illustrated in

177   Fig. S3, where V_0 stands for the initial volume of the titrimetric suspension; and V_a

178   and V_b represent the total volume of acid and alkaline solution added at each titration

179   point, respectively. In the Gran plots, the OH^- added to a suspension firstly neutralizes

180   the excess H^+ before V_{eb1}, then reacts with the functional group on the surface of the

8

181   sorbent between V_{eb1} and V_{eb2}, finally changes the pH after V_{eb2}. No apparent surface

182   reactions consuming OH⁻ before V_{eb1} were noted. The total concentration of reacting

183   H⁺ at each titration point (TOTH) was calculated using the following equation, where

184   C_b stands for NaOH concentration:

185
$$\mathrm{TOTH} = \frac{-(V_b - V_{eb1}) \times C_b}{V_0 + V_{at} + V_b} \quad (\mathrm{mol\ L^{-1}}),$$

186   **2.4. Adsorption experiment**

187   The adsorption edge experiments were conducted in 0.01 M NaNO$_3$ solutions to

188   investigate the adsorption of Cd onto montmorillonite, *B. subtilis* and the composite.

189   15 mL 178.0 μmol L^{-1} Cd(II) solution and 15 mL 2 g L^{-1} adsorbent suspensions were

190   added to 50 mL centrifuge tubes. A suitable volume of concentrated HNO$_3$ or NaOH

191   solutions was added to adjust the pH of the suspensions from 3 to 8. The final

192   concentration of Cd and adsorbents were 89.0 μmol L^{-1} and 1 g L^{-1}, respectively.

193   Fixed pH isotherm experiments were performed at pH 6 and 8 in 0.01 M NaNO$_3$

194   electrolyte. The initial concentrations of Cd ranged from 8.9–89.0 μmol L^{-1} with a

195   sorbent concentration of 1 g L^{-1}. The mixtures were allowed to equilibrate for two

196   hours at 28 ℃. After equilibration, the final suspensions were centrifuged at 12557 g

197   for 5 min, and the clear supernate was analyzed using atomic adsorption spectroscopy

198   (AAS; Varin AAS240FS) to determine the residue Cd.

199   Solution speciation of 89.0 μmol L^{-1} Cd(II) in 0.01M NaNO$_3$ was calculated as a

200   function of pH using the geochemical software Visual MINTEQ 3.1. Cd^{2+} was

201   determined to be the main species at the experimental conditions. Cd(OH)$_2$, CdOH$^+$,

202 and Cd_2OH^{3+} were also found at pH > 7.8, but in relatively small percentages.

2.5. X-ray absorption spectroscopy

204 We selected pH 6 sample of the adsorption edge experiments in section 2.4 as

205 representative to perform the XAS experiments. The solid phases after centrifugation

206 were transformed immediately to collect XAS spectra in 12 h. The sample holders

207 were packed together with moist tissues (stored at ~ -4°C) to minimize sample drying

208 during shipment to the Shanghai Synchrotron Radiation Facility (SSRF), China. The

209 X-ray absorption data at the Cd K-edge (~26700 keV) of the samples were recorded at

210 room temperature in the fluorescent mode with silicon drift fluorescence detector. The

211 station was operated with a Si(III) double crystal monochromator. During the

212 measurement, the synchrotron was operated at energy of 3.5 GeV and a current

213 between 150–210 mA. EXAFS spectra were collected from 26511 to 27551 eV.

214 Background subtraction and normalization of the XAS data were conducted in

215 ATHENA, a program in the IFEFFIT package (Ravel and Newville, 2005). The

216 background subtraction was performed using PySpline. The pre-edge was fit to a

217 linear function and the post-edge background to two 2nd-order polynomial segments.

218 To obtain information on the partitioning of Cd between the different fractions of the

219 composites, the spectra were fitted using a linear combination fitting procedure (LCF).

220 Cd-adsorbed montmorillonite, Cd-bacteria were used as end-member for the

221 2-component fitting of the binary composites, with linear combination performed over

222 the k^3-range of 2.3-10 Å^{-1} (force weight to sum to 1). The goodness of the fitting was

223 evaluated by the best-fit criterion values (R) (Du et al., 2016).

2.6. Surface complexation modeling

The program FITEQL 4.0 was utilized to determine functional group site concentrations, proton, and metal binding stability constants (Herbelin and Westall, 1999). A constant capacitance model was implemented (Tertre et al., 2006). The activity coefficient correction was made within FITEQL using the Davies equation. An indicator of the goodness of the fitting is the overall variance, V, in Y (Herbelin and Westall, 1999). $V_Y = \dfrac{WSOS}{DF}$, where WSOS is the weighted sum of squares of the residuals and DF is the degrees of freedom. Lower V_Y values signify better fits. The systematic process of developing the SCM was started by fitting the model to the experimental data for montmorillonite and *B. subtilis*.

The potentiometric titration data was fit to generate the acid-base constants and surface site densities (Fig. S4). Acid-base reactions on the surface of montmorillonite are represented by the following equations:

$$SOH \Leftrightarrow SO^- + H^+ \tag{1}$$

$$SOH + H^+ \Leftrightarrow SOH_2^+ \tag{2}$$

$$WOH \Leftrightarrow WO^- + H^+ \tag{3}$$

$$X^- + H^+ \Leftrightarrow XH \tag{4}$$

$$X^- + Na^+ \Leftrightarrow XNa \tag{5}$$

where SOH and WOH are aluminol and silanol sites on the surface of montmorillonite, respectively. X^- is the negative exchange site that can react with both H^+ and Na^+. The total concentration of exchange site and the binding stability constants of XH, XNa were used as fixed input parameters when the titration data

11

246   were fitted. These three values were 8.7×10^{-4} mol g^{-1}, -2.2 and 1.4, respectively (Table

247   S1), which come from Tertre et al. (2006) and Soltermann et al. (2014). The acid-base

248   constant and the site density of SOH and WOH were set as iterated parameters, in

249   addition, these parameters were iterated simultaneously.

250   The acid-base reactions on the surface of *B. subtilis* were represented by

251         $R\text{-}L_iH^0 \Leftrightarrow R\text{-}L_i^- + H^+$ (6)

252   where R represents the bacterium to which each functional group is attached.

253   Carboxyl sites, phosphate sites, and hydroxyl sites were considered to be the main

254   functional groups on the surface of *B. subtilis* (Yee and Fein, 2001). L_iH^0 represents

255   these three groups.

256   Acid-base equilibrium constants and site densities (Tables S1 and S2) were used

257   as fixed input parameters in the modeling of the Cd pH adsorption edge and fixed pH

258   isotherm data. The constants of Cd complexes with the functional groups on each

259   sorbent were iterated simultaneously. The following equilibria were used to describe

260   Cd(II) adsorption onto montmorillonite:

261         $2X^- + Cd^{2+} \Leftrightarrow X_2Cd$ (7)

262         $SOH + Cd^{2+} \Leftrightarrow SOCd^+ + H^+$ (8)

263   Due to their higher pK_a, hydroxyl sites are not deprotonated over the range of pH 3 to

264   8. To simplify the model, hydroxyl sites were not invoked. Cd(II) adsorption on *B.*

265   *subtilis* was described with the following reaction equilibria:

266

267     $R\text{-}COO^- + Cd^{2+} \Leftrightarrow R\text{-}COOCd^+$ (9)

268     $R\text{-}PO^- + Cd^{2+} \Leftrightarrow R\text{-}POCd^+$ (10)

269   Finally, we combined the model of Cd(II) adsorption on montmorillonite and *B.*

270   *subtilis* to simulate the adsorption behavior of Cd(II) on the composite. End-number

271   montmorillonite and *B. subtilis* models were combined in FITEQL 4.0 using the CA

272   approach.

273

274   ## 3. Results

275

276   ### 3.1. Zeta potential

277   The zeta potential of montmorillonite, *B. subtilis,* and montmorillonite–*B.*

278   *subtilis* composite are given in Fig. 1. Over the whole pH range studied, both

279   montmorillonite and the composite had negative surface charge with very low pH_{pzc}

280   around pH 3.1. The bacteria displayed a negative surface charge at pH > 3.5 and had a

281   higher pH_{pzc} than the value reported by Fein et al. (2005) ($pH_{pzc} < 2$). The negative

282   electrokinetic charge of all sorbents increased with pH and remained constant when

283   pH was higher than 5. The zeta potential of montmorillonite and bacteria were -2.29

284   mV and 12.27 mV at pH 3, -26.70 mV and -19.46 mV at pH 8. The surface of the

285   montmorillonite–bacteria composite was more negatively charged than that of

286   montmorillonite and *B. subtilis* at pH > 5, the zeta potential of the composite was

287   -20.30 mV at pH 3.

288   ### 3.2. Cadmium adsorption

289   Figure 2 shows the pH dependence of Cd adsorption on montmorillonite, *B.*

290 *subtilis*, and montmorillonite–*B. subtilis* composite. Adsorption onto montmorillonite

291 increased slowly over the pH ranges, and about 55% of the total Cd(II) was adsorbed

292 at pH 8. Adsorption onto *B. subtilis* increased sharply between pH 3 and 7 and then

293 reached a plateau at pH 7–8. Nearly 90% of total Cd(II) was adsorbed at pH 8. In

294 comparison to bacteria, the uptake of Cd on montmorillonite–*B. subtilis* composite

295 increased more slightly over the range of pH 3 to 8. The extent of adsorption onto the

296 composite increased swiftly from pH 3 to 5, and varied slightly at pH 5–8. About 60%

297 of the total Cd(II) ions were adsorbed onto the composite at pH 8.

298 **3.3. Modeling of Cd adsorption onto montmorillonite and *B. subtilis***

299 The titration data for montmorillonite and *B. subtilis* are presented in Fig. S4.

300 Bacteria exhibited significant buffering capacity over the range of pH 3 to 8.5, which

301 was assigned to the deprotonation of functional groups on cell walls (Borrok et al.,

302 2004; Moon and Peacock, 2011; Yee and Fein, 2001). Montmorillonite presented

303 strong buffering capacity only at pH < 4 and pH > 7.5. This result was in line with the

304 report of Ikhsan et al. (2005), which also showed similar buffering behaviors of a

305 Ca-montmorillonite over these pH ranges. The titration data of montmorillonite and *B.*

306 *subtilis* were successfully modeled with reactions (1)–(5) and (6). The protonation

307 constants and site densities of sorbents calculated from titration data are indicated in

308 Tables S1 and S2.

309 Adsorption of Cd onto the surface of montmorillonite and *B. subtilis* were

310 successfully modeled with reactions (7)–(10). The best-fit for cadmium adsorption on

311 montmorillonite is depicted in Fig. S5 (a). The adsorption of Cd(II) onto

14

312 montmorillonite was modeled using two adsorbed species, X_2Cd and $SOCd^+$. The

313 calculated complex stability constants of these two species were 8.30 and -1.68,

314 respectively (Table S1). The complexation of Cd(II) onto two X^- sites (X_2Cd)

315 dominated at pH < 4.5 while monodentate complexation onto SOH sites of the crystal

316 edges ($SOCd^+$) predominated at pH > 4.5. The V_Y value of the model which describes

317 the Cd adsorption on montmorillonite was 5.6. The best-fit model for the Cd

318 adsorption onto *B. subtilis* is presented in Fig. S5 (b). The optimized $logK_{R-COOCd+}$ and

319 $logK_{RPOCd+}$ values were 2.54 and 2.87, respectively (Table S2). Surface complexation

320 model successfully simulated the adsorption edge of *B. subtilis* over the pH ranges of

321 3 to 8. The model predicted that one inner-sphere monodentate complexation

322 ($R-COOCd^+$) dominated at low pH while another inner-sphere monodentate

323 complexation ($R-POCd^+$) dominated at high pH. The V_Y value of the model which

324 described the Cd adsorption on bacteria was 3.8.

325 **3.4. Modeling of Cd adsorption onto montmorillonite–*B. subtilis* composite**

326 The parameters for the model of Cd adsorption onto montmorillonite–*B. subtilis*

327 composite are shown in Table 1. As per the CA approach, the constants for

328 protonation and the acid-base reactions on the surface of the composite were the same

329 as those for the end-member montmorillonite and *B. subtilis*. The operational site

330 densities of functional groups used in the model of Cd sorption on the composite were

331 calculated   based   on   the   end-member   site   densities   weighted   to   the

332 montmorillonite:bacteria mass ratio (Moon and Peacock, 2013). The specific

333 capacitance and surface area were calculated in the same way. Four Cd complexation

species were considered in the model of Cd sorption on the composite, i.e., X_2Cd and

$SOCd^+$ on montmorillonite; two inner-sphere complexes on bacteria. The

complexation constants of the four species were the same as those optimized by the

models of Cd adsorption on montmorillonite and *B. subtilis*.

The adsorption behavior of Cd on montmorillonite–*B. subtilis* composite was

well described by CA-SCM, except some deviations were observed at pH < 5 (Fig. 3,

V_Y=15.4). The complex X_2Cd dominated below pH 4. At pH 4.5, the $SOCd^+$ was the

major species with deprotonation of the SOH surface sites. At pH 3–5.5, the

inner-sphere complex $R-COOCd^+$ on the surface of bacteria contributed 10–20% of

the total Cd adsorption. At pH above 5.5, the inner-sphere complex on the bacterial

surface ($R-POCd^+$) played an important role and amounted to 10–20% of the total Cd

adsorption. The CA-SCM provided an adequate fit to the adsorption isotherms of Cd

on the composite at pH 6 and pH 8, with V_Y values of 4.3 and 2.4, respectively (Fig.

S6). Figure 4 depicts the distribution of the total adsorbed Cd between the composite

fractions. Montmorillonite played a dominating role in Cd sorption on the composite

over the whole pH range studied. The percentage for the adsorption of Cd on

montmorillonite and *B. subtilis* in the composite at pH 6 was 71.4% and 28.6%,

respectively. The V_Y value ranging from 0.1 to 20 can generally be considered a good

fit. Overall, within the constructs of FITEQL SCM, CA-SCM is adequate to describe

the Cd adsorption behavior on the surface of the composite.

3.5. Distribution of Cd on montmorillonite–*B. subtilis* composite by XAS.

Since the model successfully described Cd adsorption on bacteria-clay composite

356   at pH > 5, herein we selected pH 6 samples to investigate whether model predictions

357   match well with the EXAFS prediction. Linear combination fitting (LCF) procedure

358   has been successfully applied to obtain the partitioning of metal adsorption on

359   bacteria-mineral composites (Du et al., 2016; Moon and Peacock, 2012; Templeton et

360   al., 2003). This approach is based on the intermediate adsorption behavior of metals

361   between the end-member components. The Cd K-edge (EXAFS) spectra of

362   montmorillonite, *Bacillus subtilis* and their composite are shown in Fig. 5. A few

363   differences between the spectrum of mineral and bacteria are pronounced at k-values

364   of 6-10 $Å^{-1}$. We were able to produce excellent fits to the Cd-composite spectra with a

365   linear combination of Cd-adsorbed montmorillonite and Cd-adsorbed *B. subtilis*

366   clusters (R-factor < 0.1). Linear combination results for the distribution of total

367   adsorbed Cd by the composite yielded a ratio of 69.1%:30.9% for montmorillonite

368   and bacterial cells, respectively. This ratio closely approaches the value obtained from

369   model speculation, which is 71.4%:28.6%.

370

371   **4. Discussions**

372   A number of investigators have employed CA-SCM to describe metal adsorption onto

373   mineral–bacteria composites (Alessi and Fein, 2010; Moon and Peacock, 2013; Song

374   et al., 2009). However, to the authors' knowledge, this is the first information on the

375   modelling of Cd adsorption by 2:1 clay mineral–bacteria composites. The species and

376   distribution of Cd on the surface of montmorillonite–*B. subtilis* composite were

377   modeled using CA-SCM in this study. Cadmium was found to be adequately

17

378   described by adsorption to the nominally assigned RCOOH and POH sites, and the X^-

379   and SOH groups on the surface of montmorillonite–*B. subtilis* composite. Our results

380   imply that all these groups have to be considered for a successful simulation of Cd

381   adsorption on 2:1 clay mineral-bacteria mixtures, compared to ferrihydrite-bacteria

382   composites where, of the bacterial component, only carboxyl (RCOOH) groups were

383   found to be responsible for heavy metal adsorption over the entire pH range studied

384   (Moon and Peacock, 2013). The model of Cd adsorption on montmorillonite–*B.*

385   subtilis composite in our study suggested that X_2Cd was the major species on the

386   composite at pH < 4. Interestingly, montmorillonite played a dominant role in Cd

387   sorption on the composite (the mass ratio of montmorillonite to bacteria was

388   87.5%:12.5%) over the entire pH range studied. However, the contribution to Cu

389   adsorption from the components of a ferrihydrite–bacteria mixture with a mass ratio

390   of 82%:18% was dependent on pH (Moon and Peacock, 2013). Bacteria and

391   ferrihydrite governed Cu adsorption at low and high pH values, respectively. The

392   montmorillonite has a permanently charged XH site, which provides a certain level of

393   adsorption capacity independent of pH, whereas the ferrihydrite-bacteria composites

394   to which the authors are contrasting their work possess only amphoteric sites (Moon

395   and Peacock, 2013). Our data revealed that the percentage of total adsorbed Cd on

396   montmorillonite in the composite was in the range of 87.3–69.1% from pH 3 to 8

397   (Figure S7). These results suggest that the bacteria fraction in the composite plays an

398   increasingly important role in the retention of cadmium ions from pH 3 to 8, although

399 slight decreases in Cd attachment were observed for the bacteria from pH 4 to 5.

400 Some of the Cd ions may have been transferred from the montmorillonite surface to

401 the bacteria in the composite with the rise of pH.

402 The modelled distribution of Cd on individual components in our

403 montmorillonite–*B. subtilis* composite was supported by the EXAFS investigations at

404 pH 6. The ratio of Cd adsorption onto montmorillonite to that of the bacterial cells

405 present in the composite as obtained from EXAFS spectra analysis closely coincides

406 with the value obtained from model speculation. Both the model simulation and

407 EXAFS observation from our study suggested that the fate of Cd is largely affected by

408 the presence of montmorillonite in soils and sediments, particularly in locations where

409 the mineral exists as the major clay mineral component. Our 2:1 clay–bacteria system

410 is different from the 1:1 clay–bacteria system reported by Alessi and Fein (2010),

411 where they found that the majority of Cd is predicted to occur onto the permanent

412 structural site of the kaolinite component only below pH 4 in a kaolinite–*B. subtilis*

413 mixture dominated by the mineral fraction (75%), and *B. subtilis* contribute nearly 58%

414 of the total reactive site. Templeton et al. (2003) reported that 71% and 29% of Pb

415 ions were adsorbed by goethite and bacteria in a goethite–bacteria composite with a

416 mass ratio of 70% : 30% at pH 7. Moon and Peacock (2012) found that the

417 distribution of Cu adsorption between ferrihydrite and bacteria fractions in a

418 ferrihydrite–bacteria composite (with a mass ratio 65% : 35%) was 80% : 20% at pH

419 6.4. Our work thus corroborates the findings of Moon and Peacock (2012) who

420   predict that, in mineral-organic composites dominated by the mineral component, the

421   mineral will be responsible for the majority of the heavy metal adsorption and the

422   composites will behave approximately additively. Moreover, this study has extended

423   their work which was based on iron (hydr)oxide-organic composites, to clay

424   mineral-organic composites. The established models from these investigations may

425   provide a universal rule to predict the behavior of trace metals in more complicated

426   ecosystems bearing mineral–organic complexes.

427   Our study provides useful insights on clay-bacteria interactions in the

428   biogeochemical interface of complex soil and its environmental consequence.

429   Although surface complexation modeling (SCM) has been widely applied to describe

430   trace metal adsorption behaviors on various soil solid components, how to apply it in

431   complex systems is still challenging. The present results indicate that Cd adsorption

432   behaviors on montmorillonite-bacteria composite is successfully described by

433   CA-SCM model, except for some deviations at pH < 5. Current SCM models might

434   be useful for the prediction of the distribution of Cd between solid and solution phases

435   in a variety of settings. Soils and various sediments are composed of clay minerals,

436   organic matter and microorganisms. It is critical to model Cd adsorption and

437   availability at the interface of multi-components interactions which is fundamental for

438   the risk evaluation of Cd-contaminated environments, especially those in temperate

439   regions such as brown clay and black clay soils which are dominated by 2:1 clays.

440   Secondly, the fact that the distribution of Cd between the end-member components is

441   dependent on pH, has important implication for Cd mobility. The adsorbed Cd

442   complexes, either outer-sphere or inner-sphere, may exhibit different exchange or

443   desorption behaviors during the changes of environmental factors, e.g., cations, redox

444   potential. The relative mobility of clay– and organic –adsorbed Cd might differ. Under

445   this premise, mineral-organic composite is a suitable analogue for a good predictor of

446   the mobility and thus eventual fate of Cd in natural environments. Lastly, our study

447   has implications for the remediation of Cd contaminant soils and sediments where 2:1

448   phyllosilicates dominate the mineral composition, in particular, when various organic

449   agents are applied, e.g., straw, manure or engineering microorganisms. These

450   substances are easily bound to soil mineral surface. In these cases, it is vital to

451   consider the fate, mobility of heavy metals with respect to mineral-organic composites,

452   in addition to pure mineral phases.

453

454 **5. Conclusions**

455   In this study, we developed surface complexation model for Cd(II) adsorption on

456   montmorillonite, *B. subtilis*, and their composite. The Cd adsorption behavior onto the

457   surface of the composite can be described by a component additivity approach

458   (CA-SCM). Underestimation was observed for the model prediction at pH < 5. The

459   X_2Cd, $SOCd^+$, $R\text{-}COOCd^+$, and $R\text{-}POCd^+$ were the predominant species of Cd

460   adsorbed on the surface of montmorillonite–*B. subtilis* composite. Montmorillonite

461   played a more important role for the binding of Cd ions in the mineral–bacteria

462   composite over the ranges of pH 3 to 8. The distribution of adsorbed Cd between the

463 montmorillonite and bacteria fractions in the montmorillonite–*B. subtilis* composite as

464 predicted by CA-SCM closely coincided the results obtained from the EXAFS spectra

465 analysis.

466

Acknowledgements

472

References

474 Akafia, M. M., Reich, T. J. and Koretsky, C. M.: Assessing Cd, Co, Cu, Ni, and Pb

475   sorption on montmorillonite using surface complexation models. Appl. Geochem.,

476   26, 154–157, 2011.

477 Alessi, D. S. and Fein, J. B.: Cadmium adsorption to mixtures of soil components:

478   Testing the component additivity approach. Chem. Geol., 270, 186–195, 2010.

479 Angove, M. J., Johnson, B. B. and Wells, J. D.: Adsorption of cadmium(II) on

480   kaolinite. Colloid Surface. A, 126, 137–147, 1997.

481 Benedicto, A., Degueldre, C. and Missana, T.: Gallium sorption on montmorillonite

482   and illite colloids: Experimental study and modelling by ionic exchange and

483   surface complexation. Appl. Geochem., 40, 43–50, 2014.

484 Borrok, D. M. and Fein, J. B.: The impact of ionic strength on the adsorption of

485   protons, Pb, Cd, and Sr onto the surfaces of Gram negative bacteria: testing

486   non-electrostatic, diffuse, and triple-layer models. J. Colloid Interface Sci., 286,

487   110–126, 2005.

488   Borrok, D., Fein, J. B. and Kulpa, C. F.: Proton and Cd adsorption onto natural

489   bacterial consortia: Testing universal adsorption behavior. Geochim. Cosmochim.

490   Ac., 68, 3231–3238, 2004.

491   Bradbury, M. H., Baeyens, B., Geckeis, H. and Rabung, T.: Sorption of

492   Eu(III)/Cm(III) on Ca-montmorillonite and Na-illite. Part 2: Surface

493   complexation modelling. Geochim. Cosmochim. Ac., 69, 5403–5412, 2005.

494   Christl, I., Milne, C. J., Kinniburgh, D. G. and Kretzschmar, R.: Relating ion binding

495   by fulvic and humic acids to chemical composition and molecular size. 2. metal

496   binding. Environ. Sci. Technol., 35, 2512–2517, 2001.

497   Chu, Z., Liu, W., Tang, H., Qian, T., Li, S., Li, Z. and Wu, G.: Surface acid-base

498   behaviors of Chinese loess. J. Colloid Interface Sci., 252, 426–32, 2002.

499   Daughney, C. J., Fowle, D. A. and Fortin, D.: The effect of growth phase on proton

500   and metal adsorption by *Bacillus subtilis*. Geochim. Cosmochim. Ac., 65,

501   1025–1035, 2001.

502   Dong, W. and Wan, J.: Additive surface complexation modeling of uranium(VI)

503   adsorption onto quartz-sand dominated sediments. Environ. Sci. Technol., 48,

504   6569–77, 2014.

505   Du, H., Chen, W., Cai, P., Rong, X., Dai, K., Peacock, C. L. and Huang, Q.: Cd(II)

506   sorption on montmorillonite-humic acid-bacteria composites. Sci. Rep., 6, 19499,

507   2016.

508   Du, Q., Sun, Z. X., Forsling, W. and Tang, H. X.: Acid–base properties of aqueous

509   illite surfaces. J. Colloid Interface Sci., 187, 221–231, 1997.

510   Fein, J. B., Fowle, D. A., Daughney, C. J., Yee, N. and Davis, T. A.: A chemical

511   equilibrium model for metal adsorption onto bacterial surfaces. Geochim.

512   Cosmochim. Ac., 61, 3319–3328, 1997.

513   Fein, J. B., Boily, J. F. and Yee, N.: Gorman-Lewis, D.; Turner, B. F., Potentiometric

514   titrations of *Bacillus subtilis* cells to low pH and a comparison of modeling

515   approaches. Geochim. Cosmochim. Ac., 69, 1123–1132, 2005.

516   Fomina, M. and Gadd, G. M.: Biosorption: current perspectives on concept, definition

517   and application. Bioresour. Technol., 160, 3–14, 2014.

518   Fowle, D. A. and Fein, J. B.: Competitive adsorption of metal cations onto two gram

519   positive bacteria: Testing the chemical equilibrium model. Geochim. Cosmochim.

520   Ac., 63, 3059–3067, 1999.

521   Gustafsson, J. P., Persson, I., Oromieh, A. G., van Schaik, J. W., Sjostedt, C. and

522   Kleja, D. B.: Chromium(III) complexation to natural organic matter: mechanisms

523   and modeling. Environ. Sci. Technol., 48, 1753–61, 2014.

524   He, J. and Chen, J. P.: A comprehensive review on biosorption of heavy metals by

525   algal biomass: materials, performances, chemistry, and modeling simulation tools.

526   Bioresour. Technol., 160, 67–78, 2014.

527   Herbelin, A. L. and Westall, J. C.: FITEQL:a computer program for the determination

528   of chemical equilibrium constants from experimental data. Report. 94-01.

529   Department of Chem, Oregon State University, Corvallis, 1999.

530   Hong, Z., Chen,W., Rong, X., Cai, P., Dai, K. and Huang, Q.: The effect of

531   extracellular polymeric substances on the adhesion of bacteria to clay minerals

532   and goethite. Chem. Geol., 360-361, 118–125, 2013.

533   Hong, Z., Rong, X., Cai, P., Dai, K., Liang, W., Chen, W. and Huang, Q.: Initial

534   adhesion of *Bacillus subtilis* on soil minerals as related to their surface properties.

535   Eur. J. Soil. Sci., 63, 457–466, 2012.

536   Ikhsan, J., Wells, J. D., Johnson, B. B. and Angove, M. J.: Surface complexation

537   modeling of the sorption of Zn(II) by montmorillonite. Colloid Surface. A, 252,

538   33–41, 2005.

539   Kenney, J. P. and Fein, J. B.: Cell wall reactivity of acidophilic and alkaliphilic

540   bacteria determined by potentiometric titrations and Cd adsorption experiments.

541   Environ. Sci. Technol., 45, 4446–4452, 2011.

542   Kim, S. S., Min, J. H., Lee, J. K., Baik, M. H., Choi J. W. and Shin, H. S.: Effects of

543   pH and anions on the sorption of selenium ions onto magnetite. J. Environ.

544   Radioact., 104, 1–6, 2012.

545   Koopal, L. K., Saito, T., Pinheiro, J. P. and van Riemsdijk, W. H.: Ion binding to

546   natural organic matter: General considerations and the NICA–Donnan model.

547   Colloid Surface. A, 265, 40–54, 2005.

548   Lackovic, K., Angove, M. J., Wells, J. D. and Johnson, B. B.: Modeling the

549   adsorption of Cd(II) onto goethite in the presence of citric acid. J. Colloid

550   Interface Sci., 269, 37–45, 2004a.

551   Lackovic, K., Wells, J. D., Johnson, B. B. and Angove, M. J.: Modeling the

552   adsorption of Cd(II) onto kaolinite and Muloorina illite in the presence of citric

553   acid. J. Colloid Interface Sci., 270, 86–93, 2004b.

554   Landry, C. J., Koretsky, C. M., Lund, T. J., Schaller, M. and Das, S.: Surface

555   complexation modeling of Co(II) adsorption on mixtures of hydrous ferric oxide,

556   quartz and kaolinite. Geochim. Cosmochim. Ac., 73, 3723–3737, 2009.

557   Liu, R. X., Song, Y. H. and Tang, H. X.: Application of the surface complexation

558   model to the biosorption of Cu(II). Adsorpt. Sci. Technol., 31, 1–16, 2013.

559   Liu, W. X., Sun, Z. X., Forsling, W., Du, Q. and Tang, H. X.: A comparative study of

560   surface acid-base characteristics of natural illites from different origins. J. Colloid

561   Interface Sci., 219, 48–61, 1999.

562   Milne, C. J., Kinniburgh, D. G., van Riemsdijk, W. H. and Tipping, E.: Generic

563   NICA-Donnan model parameters for metal-ion binding by humic substances.

564   Environ. Sci. Technol., 37, 958–971, 2003.

565   Moon, E. M. and Peacock, C. L.: Adsorption of Cu(II) to *Bacillus subtilis*: A

566   pH-dependent EXAFS and thermodynamic modelling study. Geochim.

567   Cosmochim. Ac., 75, 6705–6719, 2011.

568   Moon, E. M. and Peacock, C. L.: Adsorption of Cu(II) to ferrihydrite and

569　　　ferrihydrite–bacteria composites: Importance of the carboxyl group for Cu

570　　　mobility in natural environments. Geochim. Cosmochim. Ac., 92, 203–219, 2012.

571　Moon, E. M. and Peacock, C. L.: Modelling Cu(II) adsorption to ferrihydrite and

572　　　ferrihydrite–bacteria composites: Deviation from additive adsorption in the

573　　　composite sorption system. Geochim. Cosmochim. Ac., 104, 148–164, 2013.

574　Ravel, B. and Newville, M.: ATHENA, ARTEMIS, HEPHAESTUS: data analysis for

575　　　X-ray absorption spectroscopy using IFEFFIT. J. Synchrotron Radiat., 12,

576　　　537–541, 2005.

577　Reich, T. J., Das S., Koretsky, C. M., Lund, T. J. and Landry, C. J.: Surface

578　　　complexation modeling of Pb(II) adsorption on mixtures of hydrous ferric oxide,

579　　　quartz and kaolinite. Chem. Geol., 275, 262–271, 2010.

580　Soltermann, D., Baeyens, B., Bradbury, M. H. and Fernandes, M. M.: Fe(II) uptake on

581　　　natural montmorillonites. II. surface complexation modeling. Environ. Sci.

582　　　Technol., 48, 8698–705, 2014.

583　Song, Y. T., Swedlund, P., Singha, N. and Swift, S.: Cadmium(II) speciation in

584　　　complex aquatic systems: A study with ferrihydrite, bacteria, and an organic

585　　　Ligand. Environ. Sci. Technol., 43, 7430–7436, 2009.

586　Templeton, A. S., Spormann, A. M. and Brown, G. E.: Speciation of Pb(II) Sorbed by

587　　　*Burkholderia cepacia*/Goethite Composites. Environ. Sci. Technol., 37,

588　　　2166–2172, 2003.

589　Tertre, E., Castet, S., Berger, G., Loubet, M. and Giffaut, E.: Surface chemistry of

590   kaolinite and Na-montmorillonite in aqueous electrolyte solutions at 25 and 60 ℃:

591   Experimental and modeling study. Geochim. Cosmochim. Ac., 70, 4579–4599,

592   2006.

593   Tournassat, C., Neaman, A., Villieras, F., Bosbach, D. and Charlet, L.:

594   Nanomorphology of montmorillonite particles: Estimation of the clay edge

595   sorption site density by low-pressure gas adsorption and AFM observations. Am.

596   Mineral., 88, 1989–1995, 2003.

597   Wang, Z. and Giammar, D. E.: Mass action expressions for bidentate adsorption in

598   surface complexation modeling: theory and practice. Environ. Sci. Technol., 47,

599   3982–96, 2013.

600   Wang, Z., Lee, S. W., Catalano, J. G., Lezama-Pacheco, J. S., Bargar, J. R., Tebo, B.

601   M. and Giammar, D. E.: Adsorption of uranium(VI) to manganese oxides: X-ray

602   absorption spectroscopy and surface complexation modeling. Environ. Sci.

603   Technol., 47, 850–858, 2013.

604   Weng, L. P., Van Riemsdijk, W. H. and Hiemstra, T.: Cu^{2+} and Ca^{2+} adsorption to

605   goethite in the presence of fulvic acids. Geochim. Cosmochim. Ac., 72,

606   5857–5870, 2008.

607   Yee, N. and Fein, J. B.: Cd adsorption onto bacterial surfaces: A universal adsorption

608   edge? Geochim. Cosmochim. Ac., 65, 2037–2042, 2001.

Figure Captions

Figure 1. Zeta potential of montmorillonite, *B. subtilis*, and montmorillonite–*B. subtilis* composite at different pH values.

Figure 2. Adsorption of Cd(II) to montmorillonite, *B. subtilis*, and montmorillonite–*B. subtilis* composite as a function of pH in the presence of 0.01 M NaNO$_3$ (symbols are data points and lines are model fits). The sorbent and initial Cd concentration is 1 g L^{-1} and 10 ppm, respectively.

Figure 3. Speciation diagrams for Cd (II) adsorption onto montmorillonite–*B. subtilis* composite at 28 ℃ in the presence of 0.01 M NaNO$_3$, calculated from the surface complexation models (filled squares represent the experimental adsorption data). Cd(II) :10 ppm, composite: 0.875 g L^{-1} Mont +0.125 g L^{-1} *B. subtilis*.

Figure 4. Distribution of the total adsorbed Cd between montmorillonite and *B. subtilis* fractions in the composite predicted by CA-SCM (symbols are data points, lines are model fits) at 28 ℃ in the presence of 0.01 M NaNO$_3$. Cd(II) :10 ppm, composite : 0.875 g L^{-1} Mont +0.125 g L^{-1} *B. subtilis*.

Figure 5. Normalized Cd K-edge k^3-weighted EXAFS spectra of *B. subtilis* (a), montmorillonite (b) and montmorillonite–*B. subtilis* composite (c) at pH 6. Dotted (blue) line display the best 2-component linear combination fit.

Figure 6. Schematic cartoon illustrating Cd binding on clay-bacteria composite.

Table 1 Surface complexation model parameters for Cd(II) sorption on
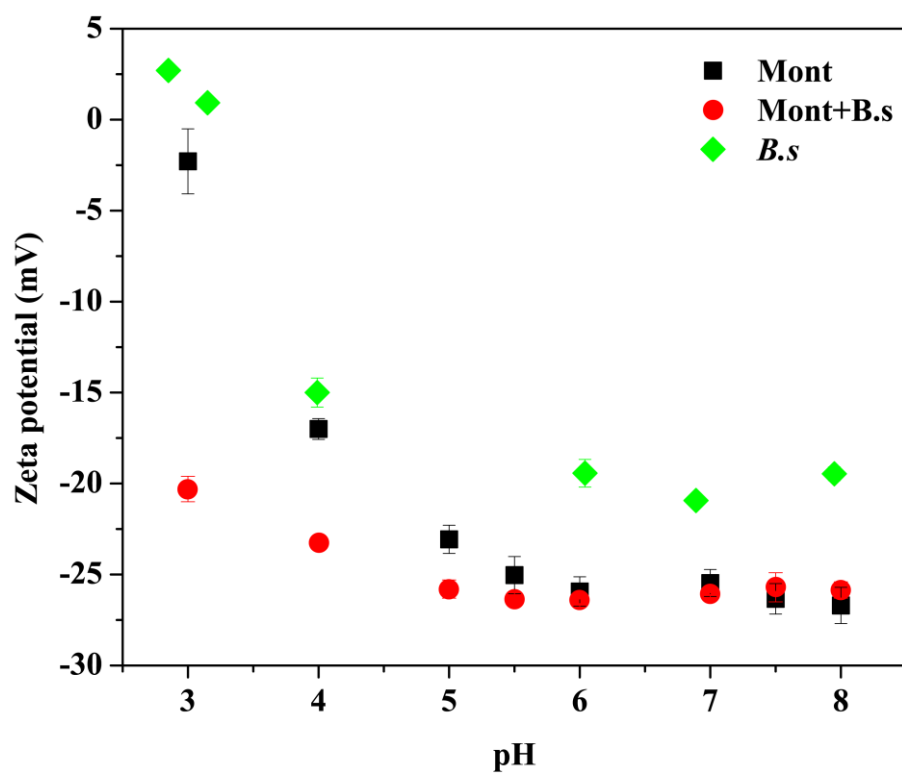
montmorillonite–*B. subtilis* composite.

Surface area (m^2/g)		422.6 [b]
Total concentration of sites (mmol/g)		
SOH		0.13 [b]
WOH		0.50 [b]
X$^-$		0.37 [b]
R-COOH		0.09 [b]
R-POH		0.07 [b]
Specific capacitance (F/m^2)		5.54 [b]
Surface reactions		
$LogK_{XH}$	$X^- + H^+ \Leftrightarrow XH$	-2.2 [a]
$LogK_{XNa}$	$X^- + Na^+ \Leftrightarrow XNa$	1.4 [a]
$LogK_{SO^-}$	$SOH \Leftrightarrow SO^- + H^+$	-4.83±0.06 [a]
$LogK_{SOH2^+}$	$SOH + H^+ \Leftrightarrow SOH_2^+$	1.86±0.06 [a]
$LogK_{WO^-}$	$WOH \Leftrightarrow WO^- + H^+$	-8.36±0.08 [a]
$LogK_{R-COO^-}$	$R\text{-}COOH \Leftrightarrow R\text{-}COO^- + H^+$	-3.32±0.08 [a]
$LogK_{R-PO^-}$	$R\text{-}POH \Leftrightarrow R\text{-}PO^- + H^+$	-5.38±0.02 [a]
$LogK_{X2Cd}$	$2X^- + Cd^{2+} \Leftrightarrow X_2Cd$	8.30±0.04 [a]
$LogK_{SOCd^+}$	$SOH + Cd^{2+} \Leftrightarrow SOCd^+ + H^+$	-1.68±0.005 [a]
$LogK_{R-COOCd^+}$	$R\text{-}COO^- + Cd^{2+} \Leftrightarrow R\text{-}COOCd^+$	2.54±0.005 [a]
$LogK_{R-POCd^+}$	$R\text{-}PO^- + Cd^{2+} \Leftrightarrow R\text{-}POCd^+$	2.87±0.02 [a]

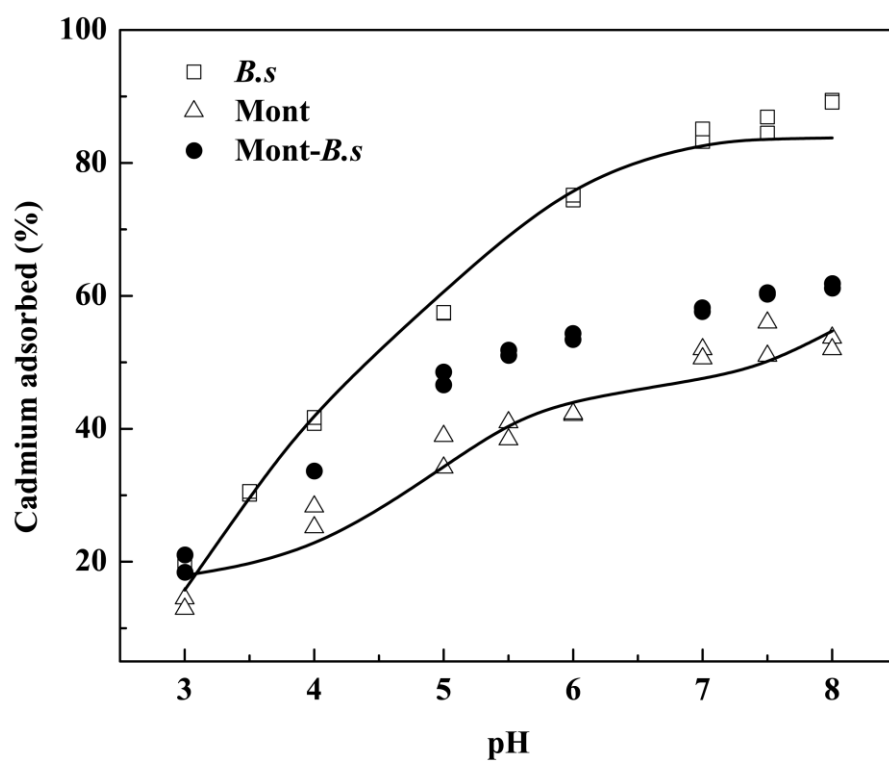[a] Fixed at those determined for montmorillonite-bacteria composite (obtained from Tables S1 and S2)

[b] Calculated using the surface site densities or surface areas or the specific capacitance of the end-member montmorillonite and *B. subtilis* weighted to the mineral:bacteria mass ratio of 7:1.

647 **Fig. 1**

648
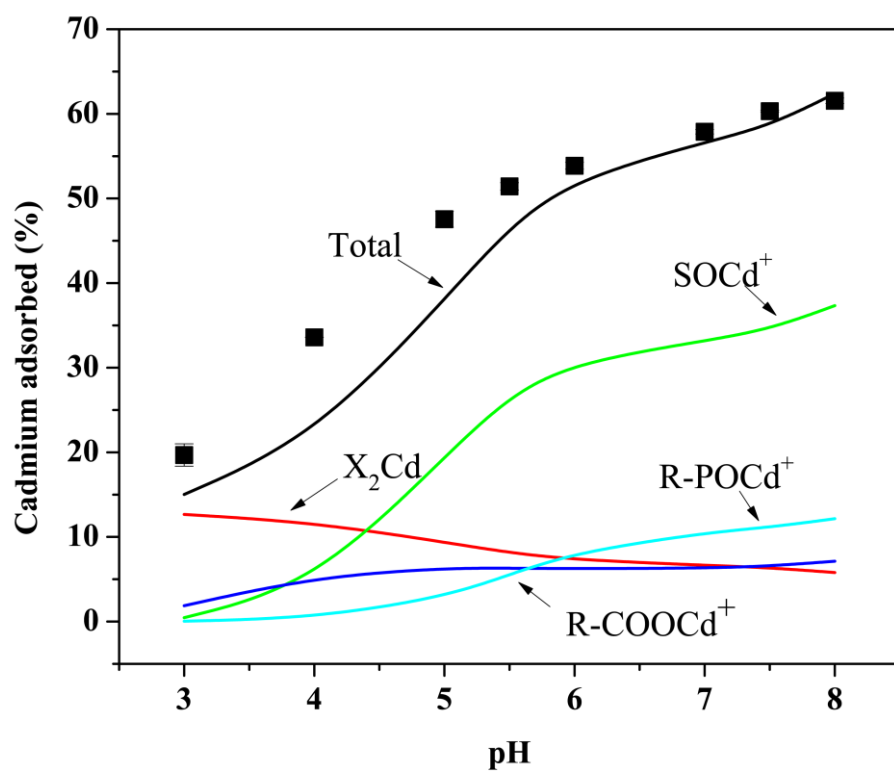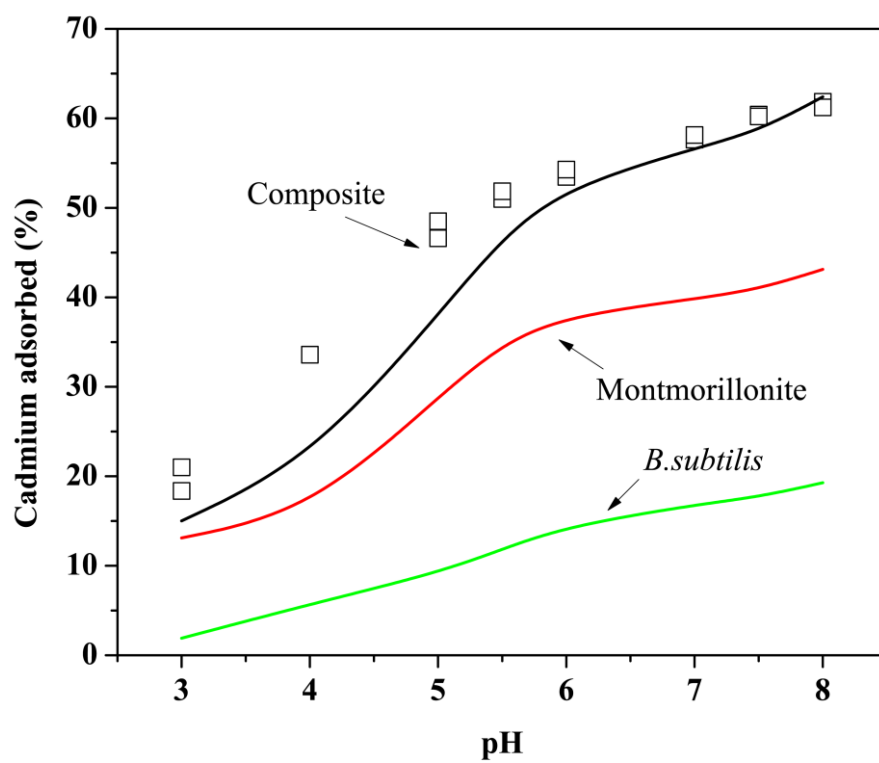649 **Fig. 2**

650
651
652
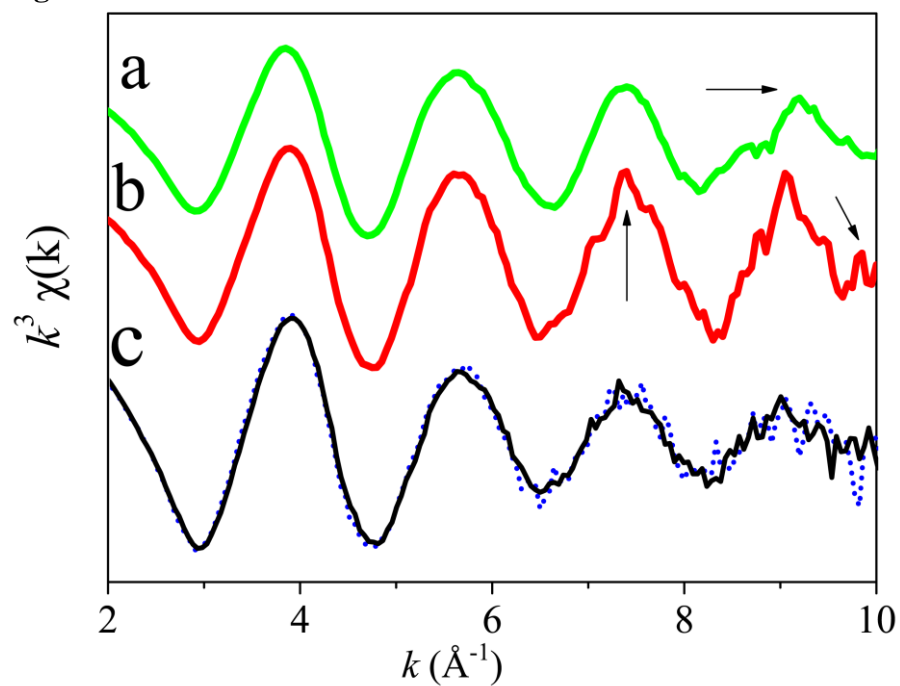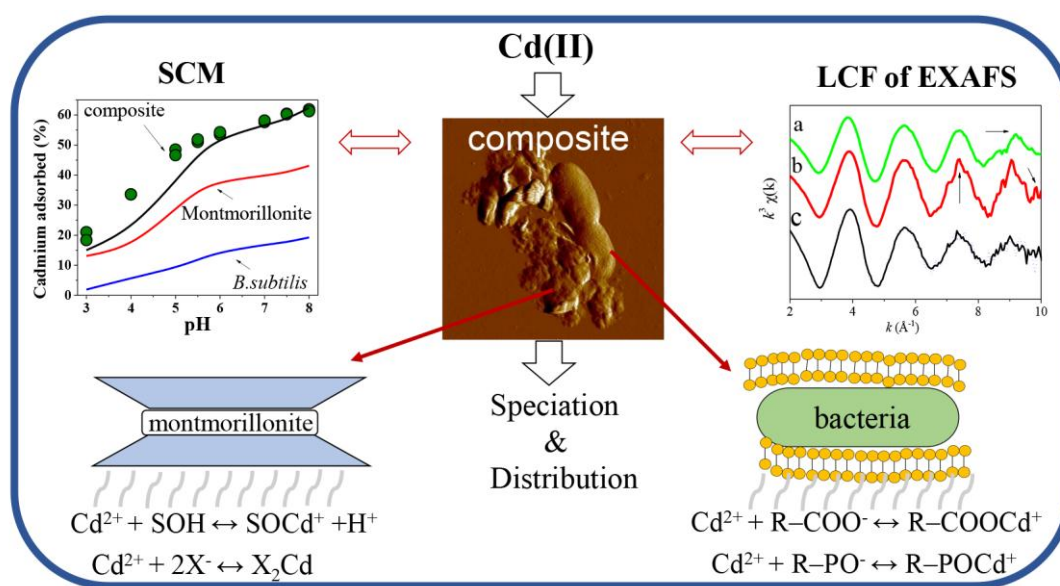653
654

655

Fig. 3

657

Fig. 4

659

660

661

662

663

Fig. 5

664

665

Fig. 6

667